

# Variational Mode Decomposition

Konstantin Dragomiretskiy and Dominique Zosso\*, *Member, IEEE*

**Abstract**—In the late nineties, Huang introduced the Hilbert-Huang transform, also known as Empirical Mode Decomposition. The goal is to recursively decompose a signal into different modes of separate spectral bands, which are unknown beforehand. The HHT/EMD algorithm is widely used today, although there is no exact mathematical model corresponding to this algorithm, and, consequently, the exact properties and limits are widely unknown. A few limitations are quite apparent, though: the algorithm is sensitive to noise and sampling. Therefore, EMD for example has difficulties separating tones of similar frequencies. Several more mathematical attempts to this decomposition problem have been made, like synchrosqueezing, empirical wavelets or recursive variational decomposition into smooth signals and residuals.

Here, we propose an entirely non-recursive variational mode decomposition model, where the modes are extracted concurrently. The model looks for a number of modes and their respective center frequencies, such that the modes reproduce the input signal, while being smooth after demodulation into baseband. In Fourier domain, this corresponds to a narrow-band prior. We show important relations to Wiener filter denoising. Indeed, the proposed method is a generalization of the classic Wiener filter into adaptive, multiple bands. Our model provides a solution to the decomposition problem that is theoretically well founded and still easy to understand. The variational model is efficiently optimized using an alternating direction method of multipliers approach. Preliminary results show excellent performance with respect to existing mode decomposition models. In particular, single harmonics can be reconstructed independently of their frequency and with precision controlled by a simple convergence tolerance criterion. Further, in contrast to EMD, the proposed VMD model is able to precisely separate any pair of harmonics, largely irrespective of their relative amplitudes and how close their frequencies are. Finally, we show promising practical decomposition results on a series of artificial and real data.

**Index Terms**—Mode decomposition, variational problem, Wiener filter, AM-FM, spectral decomposition, Hilbert transform, Fourier transform, augmented Lagrangian.

## I. INTRODUCTION

Empirical Mode Decomposition (EMD) proposed by Huang et al. [1] is an algorithmic method to detect and decompose a signal into principal “modes” - a signal with mostly compact supported Fourier spectrum. This algorithm recursively detects local minima/maxima in a signal, estimates lower/upper envelopes by spline-interpolation of these extrema, removes the average of the envelopes as “low-pass” centerline, thus isolating the high-frequency oscillations as “mode” of a signal, and continues recursively on the extracted “low-pass” centerline. In some cases, this sifting algorithm does indeed decompose a

signal into principal modes, however the resulting decomposition is highly dependent on methods of extremal point finding, interpolation of extremal points into carrier envelopes, and the stopping criteria imposed. The lack of mathematical theory and the aforementioned degrees of freedom reducing the algorithm’s robustness all leave room for theoretical development and improvement on the robustness of the decomposition [2], [3]. In some experiments it has been shown that EMD shares important similarities with wavelets and (adaptive) filter banks [4].

Despite the limited mathematical understanding and some obvious shortcomings, the EMD method, also known as the Hilbert-Huang transform (HHT), has had significant impact and is widely used in a broad variety of time-frequency analysis applications. Applications involve signal decomposition in audio engineering [5], climate analysis [6], and various flux, respiratory, and neuromuscular signals found in medicine and biology [7], [8], [9], [10], to name just a few examples.

With EMD, and in all of the previous signals, the core assumption on the individual modes is that they have compact Fourier support. In the original description, in such a mode the number of local extrema and zero-crossings differ at most by one [1]. In most related works, the definition is slightly changed into so-called *Intrinsic Mode Functions* (IMF).

**Definition** Intrinsic Mode Functions are amplitude-modulated-frequency-modulated (AM-FM) signals, written as:

$$u_k(t) = A_k(t) \cos(\phi_k(t)), \quad (1)$$

where the phase  $\phi_k(t)$  is a non-decreasing function,  $\phi'_k(t) \geq 0$ , the envelope is non-negative  $A_k(t) \geq 0$ , and, very importantly, both the envelope  $A_k(t)$  and the instantaneous frequency  $\omega_k(t) := \phi'_k(t)$  vary much slower than the phase  $\phi_k(t)$  [11], [12].

In other words, on a sufficiently long interval  $[t - \delta, t + \delta]$ ,  $\delta \approx 2\pi/\phi'_k(t)$ , the mode  $u_k(t)$  can be considered to be a pure harmonic signal with amplitude  $A_k(t)$  and instantaneous frequency  $\phi'_k(t)$  [11]. Note that the newer definition of signal components is slightly more restrictive than the original one. The immediate consequence of the IMF assumption is limited bandwidth.

Indeed, if  $\omega_k$  is the mean frequency of a mode, then its practical bandwidth increases both, with the maximum deviation of the instantaneous frequency,  $\Delta f \sim \max(|\omega_k(t) - \omega_k|)$ , and with the rate of change of the instantaneous frequency,  $f_{\text{FM}} \sim \omega'(t)$ , according to Carson’s rule:  $BW = 2(\Delta f + f_{\text{FM}})$  [13]. In addition to this comes the bandwidth of the envelope  $A_k(t)$  modulating the amplitude of the FM signal, given by its highest frequency  $f_{\text{AM}}$ . Hence we estimate the total bandwidth

\* To whom correspondence should be addressed.

This work is supported by the Swiss National Science Foundation (SNF) under grant PBELP2\_137727.

The authors are with the Department of Mathematics, University of California, Los Angeles (UCLA), Box 951555, Los Angeles, CA 90095-1555, USA, {konstantin,zosso}@math.ucla.edu.

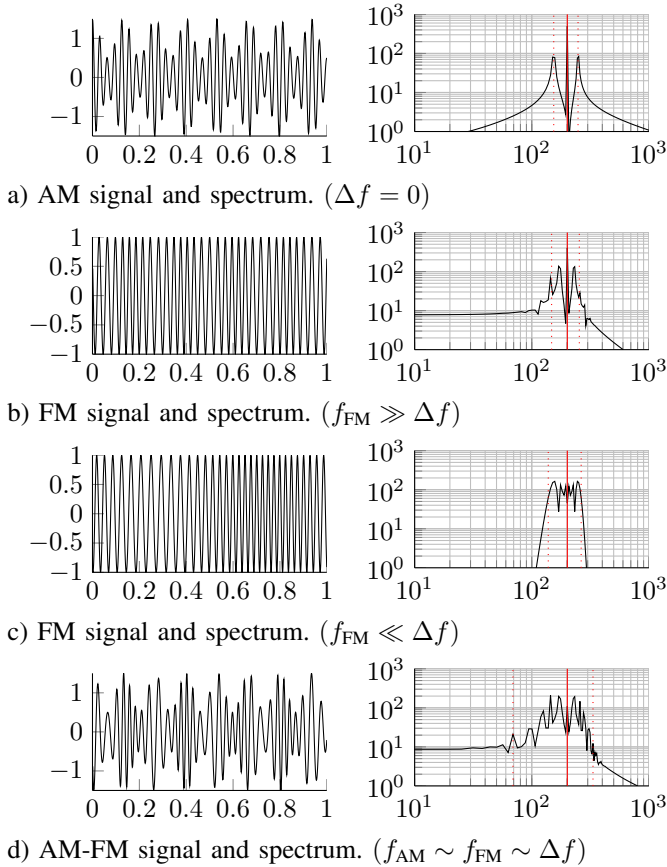


Fig. 1. AM-FM signals with limited bandwidth. Here, we use a signal  $f(t) = (1 + 0.5 \cos(2\pi f_{AM}t)) \cdot \cos(2\pi f_c t + \Delta f / f_{FM} \cos(2\pi f_{FM}t))$ . a) Pure AM signal. b) Pure FM signal with little but rapid frequency deviations. c) Pure FM signal with slow but important frequency oscillations. d) Combined AM-FM signal. The solid vertical line in the spectrum shows the carrier frequency  $f_c$ , the dotted lines correspond to the estimated band limits at  $f_c \pm BW/2$ , based on (2).

of an IMF as

$$BW = 2(\Delta f + f_{FM} + f_{AM}). \quad (2)$$

Depending on the actual IMF, either of these terms may be dominant. An illustration of four typical cases is provided in figure 1, where the last example is rather extreme in terms of required bandwidth (for illustrational purposes).

Some recent works create a partially variational approach to EMD where the signal is explicitly modeled as an IMF [14]. This method still relies on interpolation, selection of a Fourier low-pass filter, and sifting of high-frequency components. Here, the candidate modes are extracted variationally. The signal is recursively decomposed into an IMF with TV3-smooth envelope, and a TV3-smooth residual. The resulting algorithm is very similar to EMD in structure, but somewhat more robust to noise.

A slightly more variational, but still recursive decomposition scheme has been proposed in [15], for the analysis of time-varying vibration. Here, the dominant vibration is extracted by estimating its instantaneous frequency as average frequency after the Hilbert transform. Again, this process is repeated recursively on the residual signal.

An approach based on selecting appropriate wavelet scales,

dubbed *synchrosqueezing*, was proposed by Daubechies et al. [11], [16]. They remove unimportant wavelet coefficients (both in time and scale) by thresholding of the respective signal energy in that portion. Conversely, locally relevant wavelets are selected as local maxima of the continuous wavelet transform, that are shown to be tuned with the local signals, and from which the current instantaneous frequency of each mode can be recovered.

Other recent work pursuing the same goal is the Empirical Wavelet Transform (EWT) to explicitly build an adaptive wavelet basis to decompose a given signal into adaptive subbands [12]. This model relies on robust preprocessing for peak detection, then performs spectrum segmentation based on detected maxima, and constructs a corresponding wavelet filter bank. The filter bank includes flexibility for some mollification (spectral overlap), but explicit construction of frequency bands still appears slightly strict.

In this paper, we propose a new, fully intrinsic and adaptive, variational method, the minimization of which leads to a decomposition of a signal into its principal modes. Indeed, the current decomposition models are mostly limited by 1) their algorithmic ad-hoc nature lacking mathematical theory (EMD), 2) the recursive sifting in most methods, which does not allow for backward error correction, 3) the inability to properly cope with noise, 4) the hard band-limits of wavelet approaches, and 5) the requirement of predefining filter bank boundaries in EWT. In contrast, we propose a variational model that determines the relevant bands adaptively, and estimates the corresponding modes concurrently, thus properly balancing errors between them. Motivated by the narrow-band properties corresponding to the current common IMF definition, we look for an ensemble of modes that reconstruct the given input signal optimally (either exactly, or in a least-squares sense), while each being band-limited about a center frequency estimated on-line. Here, our variational model specifically can address the presence of noise in the input signal. Indeed, the tight relations to the Wiener filter actually suggest that our approach has some optimality in dealing with noise. The variational model assesses the bandwidth of the modes as H1-norm, after shifting the Hilbert-complemented, analytic signal down into baseband by complex harmonic mixing. The resulting optimization scheme is very simple and fast: each mode is iteratively updated directly in Fourier domain, as the narrow-band Wiener filter corresponding to the current estimate of the mode's center-frequency being applied to the signal estimation residual of all other modes; then the center frequency is re-estimated as the center-of-gravity of the mode's power spectrum. Our quantitative results on tone detection and separation show excellent performance irrespective of harmonic frequencies, in particular when compared to the apparent limits of EMD in this respect. Further, qualitative results on synthetic and real test signals are convincing, also regarding robustness to signal noise.

The rest of this paper is organized as follows: Section II introduces the notions of the Wiener filter, the Hilbert transform, and the analytic signal. Also, we briefly review the concept of frequency shifting through harmonic mixing. These concepts are the very building blocks of our variational mode

decomposition model. Section III presents and explains our variational model in detail, our algorithm to minimize it, and finer technicalities on boundaries, periodicity, and windowing. Section IV contains our experiments and results, namely some simple quantitative performance evaluations, and comparisons to EMD, and various synthetic multi-mode signals and our method's decomposition of them. Specifically, tone detection and separation will be analyzed and compared to that of EMD. Additionally, real signals will be considered. Section V concludes on our proposed variational mode decomposition method, including some future directions and expected improvements.

## II. TOOLS FROM SIGNAL PROCESSING

In this section we briefly review a few concepts and tools from signal processing that will constitute the building blocks of our variational mode decomposition model. First, we present a classical case of Wiener filtering for image denoising. Next, we describe the Hilbert transform and its use in the construction of a single-side band analytic signal. Finally, we show how multiplication with pure complex harmonics is used to shift the frequencies in a signal.

### A. Gaussian regularizer and Wiener filtering

Let us start with a simple denoising problem. Consider the observed signal  $f_0(t)$  to be a copy of the original signal  $f(t)$  to be recovered, affected by additive zero-mean Gaussian noise:

$$f_0 = f + \eta \quad (3)$$

Recovering the unknown signal  $f$  is a typical ill-posed inverse problem [17]. If the original signal is known to vary smoothly, one would typically write the following Tikhonov regularized minimization problem in order to estimate the noise-free signal [18], [19]:

$$\min_f \{ \|f - f_0\|_2^2 + \alpha \|\partial_t f\|_2^2 \} \quad (4)$$

This is a standard, Gaussian regularized minimum mean squares, i.e. "L2-H1" problem, of which the Euler-Lagrange equations are easily obtained as

$$f - f_0 = \alpha \partial_t^2 f. \quad (5)$$

These EL equations are typically solved in Fourier domain:

$$\hat{f}(\omega) = \frac{\hat{f}_0}{1 + \alpha\omega^2}, \quad (6)$$

where  $\hat{f}(\omega) := \mathcal{F}\{f(\cdot)\}(\omega) := 1/\sqrt{2\pi} \int_{\mathbb{R}} f(t)e^{-j\omega t} dt$ , with  $j^2 = -1$ , is the Fourier transform of the signal  $f(t)$ . Clearly, the recovered signal  $f$  is a low-pass narrow-band selection of the input signal  $f_0$  around  $\omega = 0$ . Indeed, the solution corresponds to convolution with a Wiener filter, where  $\alpha$  represents the variance of the white noise, and the signal has a lowpass  $1/\omega^2$  power spectrum prior [20], [21].

### B. Hilbert transform and analytic signal

Here, we cite the definition of the Hilbert transform given in [22]:

**Definition** The 1-D Hilbert transform is the linear, shift-invariant operator  $\mathcal{H}$  that maps all 1-D cosine functions into their corresponding sine functions. It is an all-pass filter that is characterized by the transfer function  $\hat{h}(\omega) = -j \operatorname{sgn}(\omega) = -j\omega/|\omega|$ .

Thus, the Hilbert transform is a multiplier operator in the spectral domain. The corresponding impulse response is  $h(t) = 1/(\pi t)$ . Because  $h(t)$  is not integrable the integrals defining the convolution do not converge. Instead, the Hilbert transform  $\mathcal{H}f(t)$  of a signal  $f(t)$  is therefore obtained as the Cauchy principal value (denoted p.v.) of :

$$\mathcal{H}f(t) = \frac{1}{\pi} \text{p.v.} \int_{\mathbb{R}} \frac{f(v)}{t-v} dv. \quad (7)$$

Finally, the inverse Hilbert transform is given by its negative,  $\mathcal{H}^{-1} = -\mathcal{H}$ , thus:

$$\mathcal{H}^2 f(t) = -f(t). \quad (8)$$

For further properties and analysis of the Hilbert transform, we refer e.g. to [23]. The most prominent use of the Hilbert transform is in the construction of an analytic signal from a purely real signal, as proposed by Gabor [24].

**Definition** Let  $f(t)$  be a purely real signal. The complex analytic signal is now defined as:

$$f_A(t) = f(t) + j\mathcal{H}f(t) = A(t)e^{j\phi(t)}. \quad (9)$$

This analytic signal has the following important properties. The complex exponential term  $e^{j\phi(t)}$  is a phasor describing the rotation of the complex signal in time,  $\phi(t)$  being the phase, while the amplitude is governed by the real envelope  $A(t)$ . This representation is particularly useful in the analysis of time-varying amplitude and instantaneous frequency, defined as  $\omega(t) = d\phi(t)/dt$ . The second property is the unilateral spectrum of the analytic signal, consisting only of non-negative frequencies, hence its use in single-sideband modulation. Finally, we note that from such an analytical signal, the original real signal is easily retrieved as the real part:

$$f(t) = \Re\{f_A(t)\}. \quad (10)$$

It is worthwhile highlighting the simple relations between the Fourier spectra of the real signal and its analytic counterpart, as defined by (9). First, we recall that the (Fourier) spectrum of a real signal is a Hermitian function:

$$\hat{f}(-\omega) = \overline{\hat{f}(\omega)}. \quad (11)$$

In contrast, the spectrum of the analytic signal has only non-negative frequencies. In particular:

$$\hat{f}_A(\omega) = \begin{cases} 0 & \omega < 0 \\ \hat{f}(0) & \omega = 0 \\ 2\hat{f}(\omega) & \omega > 0. \end{cases} \quad (12)$$

### C. Frequency mixing and heterodyne demodulation

The last concept that we wish to recall before introducing the proposed variational mode decomposition, is the principle of frequency mixing. Mixing is the process of combining two signals non-linearly, thus introducing cross-frequency terms in the output. The simplest mixer is multiplication. Multiplying two real signals with frequencies  $f_1$  and  $f_2$ , respectively, creates mixed frequencies in the output at  $f_1 - f_2$  and  $f_1 + f_2$ , which is easily illustrated by the following trigonometric identity:

$$2 \cos(2\pi f_1 t) \cos(2\pi f_2 t) = \cos(2\pi(f_1 + f_2)t) + \cos(2\pi(f_1 - f_2)t). \quad (13)$$

Typical applications are the heterodyne downmixing of the modulated high-frequency carrier signal with a local (heterodyne) oscillator in a radio receiver. In such devices, the selection of either of the two output terms is achieved by filtering. Here, instead of filtering the output, we mix the two respective analytic signals:

$$e^{j2\pi f_1 t} e^{j2\pi f_2 t} = e^{j2\pi(f_1 + f_2)t}, \quad (14)$$

i.e., the mixed signal is automatically “mono-tone” (constituted of a single frequency only). In Fourier terms, this is well known as the following transform pair:

$$f_A(t) e^{-j\omega_0 t} \xleftrightarrow{\mathcal{F}} \hat{f}_A(\omega) * \delta(\omega + \omega_0) = \hat{f}_A(\omega + \omega_0), \quad (15)$$

where  $\delta$  is the Dirac distribution and  $*$  denotes convolution. Thus, multiplying an analytic signal with a pure exponential results in simple frequency shifting.

## III. VARIATIONAL MODE DECOMPOSITION

In this section we introduce our proposed model for variational mode decomposition, essentially based on the three concepts outlined in the previous section.

The goal of VMD is to decompose an input signal into a discrete number of sub-signals (modes), that have specific sparsity properties while reproducing the input. Here, the sparsity prior of each mode is chosen to be its bandwidth in spectral domain. In other words, we require each mode  $k$  to be mostly compact around a center pulsation  $\omega_k$ , which is to be determined along with the decomposition.

In order to assess the bandwidth of a mode, we propose the following scheme: 1) for each mode  $u_k$ , compute the associated analytic signal by means of the Hilbert transform in order to obtain a unilateral frequency spectrum. 2) for each mode, shift the mode’s frequency spectrum to “baseband”, by mixing with an exponential tuned to the respective estimated center frequency. 3) The bandwidth is now estimated through the H1 Gaussian smoothness of the demodulated signal, i.e. the squared L2-norm of the gradient. The resulting constrained variational problem is the following:

$$\begin{aligned} \min_{u_k, \omega_k} & \left\{ \sum_k \left\| \partial_t \left[ \left( \delta(t) + \frac{j}{\pi t} \right) * u_k(t) \right] e^{-j\omega_k t} \right\|_2^2 \right\} \\ \text{s.t.} & \quad \sum_k u_k = f \end{aligned} \quad (16)$$

The reconstruction constraint can be addressed in different ways. Here, we suggest making use of both a quadratic penalty term and Lagrangian multipliers in order to render the problem unconstrained. Therefore, we introduce the augmented Lagrangian  $\mathcal{L}$  as follows [25], [26]:

$$\begin{aligned} \mathcal{L}(u_k, \omega_k, \lambda) = & \alpha \sum_k \left\| \partial_t \left[ \left( \delta(t) + \frac{j}{\pi t} \right) * u_k(t) \right] e^{-j\omega_k t} \right\|_2^2 \\ & + \left\| f - \sum_k u_k \right\|_2^2 + \left\langle \lambda, f - \sum_k u_k \right\rangle. \end{aligned} \quad (17)$$

The solution to the original minimization problem (16) is now found as the saddle point of the augmented Lagrangian  $\mathcal{L}$  in a sequence of iterative sub-optimizations called alternate direction method of multipliers (ADMM), see algorithm 1. In the next paragraphs, we detail how the respective sub-problems can be solved.

---

### Algorithm 1 ADMM optimization concept for VMD

---

Initialize  $u_k^1, \omega_k^1, \lambda^1, n \leftarrow 0$

**repeat**

$n \leftarrow n + 1$

**for**  $k = 1 : K$  **do**

Update  $u_k$ :

$$u_k^{n+1} \leftarrow \arg \min_{u_k} \mathcal{L}(u_1^{n+1}, \dots, u_{k-1}^{n+1}, u_k, u_{k+1}^n, \dots, u_K^n, \omega_1^n, \dots, \omega_K^n, \lambda^n) \quad (18)$$

**end for**

**for**  $k = 1 : K$  **do**

Update  $\omega_k$ :

$$\omega_k^{n+1} \leftarrow \arg \min_{\omega_k} \mathcal{L}(u_1^{n+1}, \dots, u_K^{n+1}, \omega_1^{n+1}, \dots, \omega_{k-1}^{n+1}, \omega_k, \omega_{k+1}^n, \dots, \omega_K^n, \lambda^n) \quad (19)$$

**end for**

Dual ascent:

$$\lambda^{n+1} \leftarrow \lambda^n + \tau \left( f - \sum_k u_k^{n+1} \right) \quad (20)$$

**until** convergence:  $\sum_k \|u_k^{n+1} - u_k^n\|_2^2 / \|u_k^n\|_2^2 < \epsilon$ .

---

#### A. Minimization w.r.t. $u_k$

To update the modes  $u_k$ , we first rewrite the subproblem (18) as the following equivalent minimization problem:

$$\begin{aligned} u_k^{n+1} = & \arg \min_{u_k \in \mathbb{R}} \left\{ \alpha \left\| \partial_t \left[ \left( \delta(t) + \frac{j}{\pi t} \right) * u_k(t) \right] e^{-j\omega_k t} \right\|_2^2 \right. \\ & \left. + \left\| f - \sum u_i + \frac{\lambda}{2} \right\|_2^2 \right\}. \end{aligned} \quad (21)$$

Making use of the Parseval/Plancherel Fourier isometry under the L2 norm, this problem can be solved in spectral domain:

$$\hat{u}_k^{n+1} = \arg \min_{\hat{u}_k, \hat{u}_k = \hat{u}_k^*} \left\{ \alpha \|j\omega [(1 + \text{sgn}(\omega + \omega_k)) \hat{u}_k(\omega + \omega_k)]\|_2^2 + \left\| \hat{f} - \sum \hat{u}_i + \frac{\hat{\lambda}}{2} \right\|_2^2 \right\}. \quad (22)$$

We now perform a change of variables  $\omega \rightarrow \omega + \omega_k$  in the first term:

$$\hat{u}_k^{n+1} = \arg \min_{\hat{u}_k, \hat{u}_k = \hat{u}_k^*} \left\{ \alpha \|j(\omega - \omega_k) [(1 + \text{sgn}(\omega)) \hat{u}_k(\omega)]\|_2^2 + \left\| \hat{f} - \sum \hat{u}_i + \frac{\hat{\lambda}}{2} \right\|_2^2 \right\}. \quad (23)$$

Exploiting the Hermitian symmetry of the real signals in the reconstruction fidelity term, we can write both terms as half-space integrals over the non-negative frequencies:

$$\hat{u}_k^{n+1} = \arg \min_{\hat{u}_k, \hat{u}_k = \hat{u}_k^*} \left\{ \int_0^\infty 4\alpha(\omega - \omega_k)^2 |\hat{u}_k(\omega)|^2 + 2 \left( \hat{f} - \sum \hat{u}_i + \frac{\hat{\lambda}}{2} \right)^2 d\omega \right\}. \quad (24)$$

The solution of this quadratic optimization problem is readily found by letting the first variation vanish for the positive frequencies:

$$\hat{u}_k^{n+1} = \left( \hat{f} - \sum_{i \neq k} \hat{u}_i + \frac{\hat{\lambda}}{2} \right) \frac{1}{1 + 2\alpha(\omega - \omega_k)^2}, \quad (25)$$

which is clearly identified as a Wiener filtering of the current residual, with signal prior  $1/(\omega - \omega_k)^2$ . The full spectrum of the real mode is then simply obtained by Hermitian symmetric completion. Conversely, the mode in time domain is obtained as the real part of the inverse Fourier transform of this filtered analytic signal.

### B. Minimization w.r.t. $\omega_k$

The center frequencies  $\omega_k$  do not appear in the reconstruction fidelity term, but only in the bandwidth prior. The relevant problem thus writes:

$$\omega_k^{n+1} = \arg \min_{\omega_k} \left\{ \left\| \partial_t \left[ \left( \delta(t) + \frac{j}{\pi t} \right) * u_k(t) \right] e^{-j\omega_k t} \right\|_2^2 \right\}. \quad (26)$$

As before, the optimization can take place in Fourier domain, and we end up optimizing:

$$\omega_k^{n+1} = \arg \min_{\omega_k} \left\{ \int_0^\infty (\omega - \omega_k)^2 |\hat{u}_k(\omega)|^2 d\omega \right\}, \quad (27)$$

This quadratic problem is easily solved as:

$$\omega_k^{n+1} = \frac{\int_0^\infty \omega |\hat{u}_k(\omega)|^2 d\omega}{\int_0^\infty |\hat{u}_k(\omega)|^2 d\omega}, \quad (28)$$

which puts the new  $\omega_k$  at the center of gravity of the corresponding mode's power spectrum. This mean carrier frequency is the frequency of a least squares linear regression to the instantaneous phase observed in the mode.

Plugging the solutions of the sub-optimizations into the ADMM algorithm 1, and directly optimizing in Fourier domain where appropriate, we get the complete algorithm for variational mode decomposition, summarized in algorithm 2.

---

### Algorithm 2 Complete optimization of VMD

---

Initialize  $\hat{u}_k^1, \omega_k^1, \hat{\lambda}^1, n \leftarrow 0$

**repeat**

$n \leftarrow n + 1$

**for**  $k = 1 : K$  **do**

Update  $\hat{u}_k$  for all  $\omega \geq 0$ :

$$\hat{u}_k^{n+1} \leftarrow \frac{\hat{f} - \sum_{i < k} \hat{u}_i^{n+1} - \sum_{i > k} \hat{u}_i^n + \frac{\hat{\lambda}^n}{2}}{1 + 2\alpha(\omega - \omega_k^n)^2} \quad (29)$$

Update  $\omega_k$ :

$$\omega_k^{n+1} \leftarrow \frac{\int_0^\infty \omega |\hat{u}_k^{n+1}(\omega)|^2 d\omega}{\int_0^\infty |\hat{u}_k^{n+1}(\omega)|^2 d\omega} \quad (30)$$

**end for**

Dual ascent for all  $\omega \geq 0$ :

$$\hat{\lambda}^{n+1} \leftarrow \hat{\lambda}^n + \tau \left( \hat{f} - \sum_k \hat{u}_k^{n+1} \right) \quad (31)$$

**until** convergence:  $\sum_k \|\hat{u}_k^{n+1} - \hat{u}_k^n\|_2^2 / \|\hat{u}_k^n\|_2^2 < \epsilon$ .

---

### C. Inexact reconstruction and denoising

Here, the role of the Lagrangian multiplier is to enforce the constraint, while the quadratic penalty improves convergence. If exact reconstruction is not required, but some slack is to be allowed, using the quadratic penalty only while dropping the Lagrangian multiplier would be the appropriate choice. Indeed, the quadratic penalty on its own represents the least-squares fidelity prior associated with additive Gaussian noise.

### D. On boundaries, periodicity, and windowing

Up until now, the signals  $f$  and the modes  $u_k$  have been considered continuous over the whole axis  $t \in \mathbb{R}$ . However, in signal processing we are much more likely to be working with signals that are both finite in time and resolution. Let us say we restrict the time window to  $t \in [0, 1]$ . Luckily the results presented so far equally hold for discrete, finite time signals, where simply the continuous Fourier transform is replaced by its discrete counterpart. The only problems arise at the boundaries of the signal.

Indeed, when considering short-time signals, the implicit assumption here is that the signal considered is just a one-period extract of an infinitely long, periodic signal. Consequently, the spectrum of a seemingly simple "general trend"-function on a short interval, say  $f : [0, 1] \mapsto \mathbb{R} : f(t) = t$ , contains an important amount of high-frequency harmonics,

since we are effectively looking at the spectrum of the periodic sawtooth function. Conversely in time domain, we realize that at the endpoints of the domain, the periodized function is discontinuous, thus severely affecting the H1 smoothing term.

There are two remedies to this. Ideally, one should exclude the boundaries of the domain in the evaluation of the smoothness, i.e. restrict its evaluation to the open interval  $(0, 1)$ . However, this clearly breaks the Parseval/Plancherel Fourier isometry and the whole beauty of the spectral solution is lost. Therefore, we suggest a less far-reaching remedy, that is classically used in short-term Fourier analysis: smooth windowing. This approach is particularly useful in cases, where the variational mode decomposition is anyway performed on short chunks of a much longer time series signal.

For simplicity, in the following examples, we will use a Gaussian window. This window is simply applied to the input signal  $f$  prior to performing the VMD algorithm. After decomposition, the individual modes can be “unwindowed” by simple division. This, however, will largely affect reconstruction fidelity close to the window borders. This is particularly apparent in the single frame decomposition. In a sliding window short-time analysis of a larger time series signal, however, instead of window division, the modes can be stitched together by simple addition without error amplification.

#### IV. EXPERIMENTS AND RESULTS

In this section, we apply the proposed VMD algorithm to a series of test signals in order to assess the validity of our approach. First, we focus on a few problems that have been successfully employed for highlighting the strengths and shortcomings of the EMD / Hilbert-Huang-Transform, namely tones versus sampling, and tones separation [2]. Then we briefly investigate noise robustness of VMD. Finally, we shift our attention to more complex signals, which have already been used in [14] and [12].

##### A. Tones and sampling

When the input signal  $f = f_\nu(t) = \cos(2\pi\nu t)$  is composed of a pure harmonic, then the mode decomposition is expected to output exactly this harmonic. As reported in [2], this does not happen to be the case with EMD, since the local extrema can suffer from important jittering with increasing frequency. In [2], the relative error

$$e(\nu) = \|f_\nu(t) - u_1(t)\|_2 / \|f_\nu(t)\|_2 \quad (32)$$

was introduced, and a quadratic increase with frequency of an upper bound to this relative error was reported for EMD. Further, EMD has pronounced spikes of near-perfect reconstruction when the sampling frequency is an even multiple of the tone’s frequency.

Here, we perform this analysis for the proposed VMD model. We refrain from windowing and consider exactly the same signals as for the EMD analysis. The results for different convergence tolerance levels  $\epsilon$  are shown in figure 2. It can be clearly seen that the relative reconstruction error is largely independent of the harmonic’s frequency. Moreover, the relative error is nicely controlled by the tolerance level  $\epsilon$ .

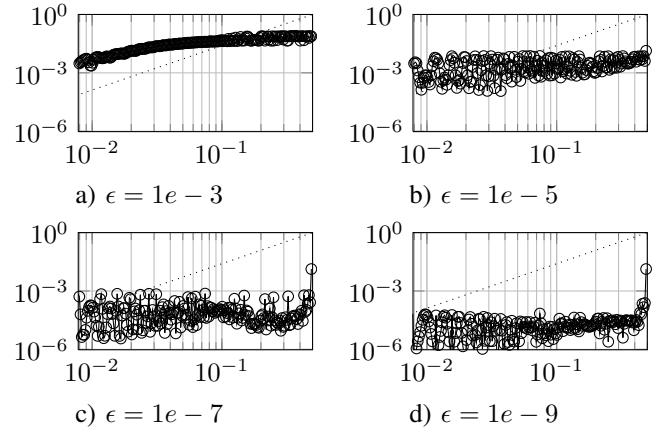


Fig. 2. Mode decomposition of a pure harmonic: Relative error for a range of 257 frequencies, for different convergence tolerance levels  $\epsilon$ . The relative error does not correlate with the tone frequency. Further, reconstruction error can be controlled by decreasing the stopping criterion’s convergence tolerance, except for frequencies very close to the Nyquist frequency. In contrast, EMD’s relative tone reconstruction error is bounded by a quadratic increase with frequency (dotted line) [2].

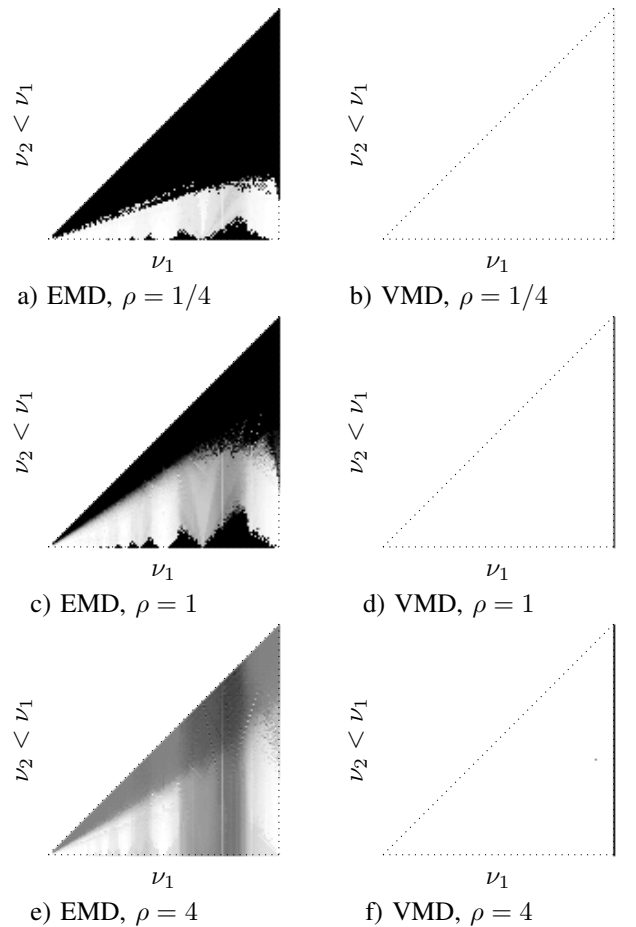


Fig. 3. Tones separation. In a superposition of two tones of frequencies  $\nu_2 < \nu_1 < f_s/2$  and equal amplitudes, the mode decompositions between EMD and VMD vary significantly. The plot indicates relative error, with values between 0 (white) and 0.5 (black). a,c,e) EMD has important areas of confusion (dark), where the tones cannot be separated correctly [2]. b,d,f) In contrast, VMD achieves good tones separation almost everywhere but for  $\nu_1$  too close to the Nyquist frequency.

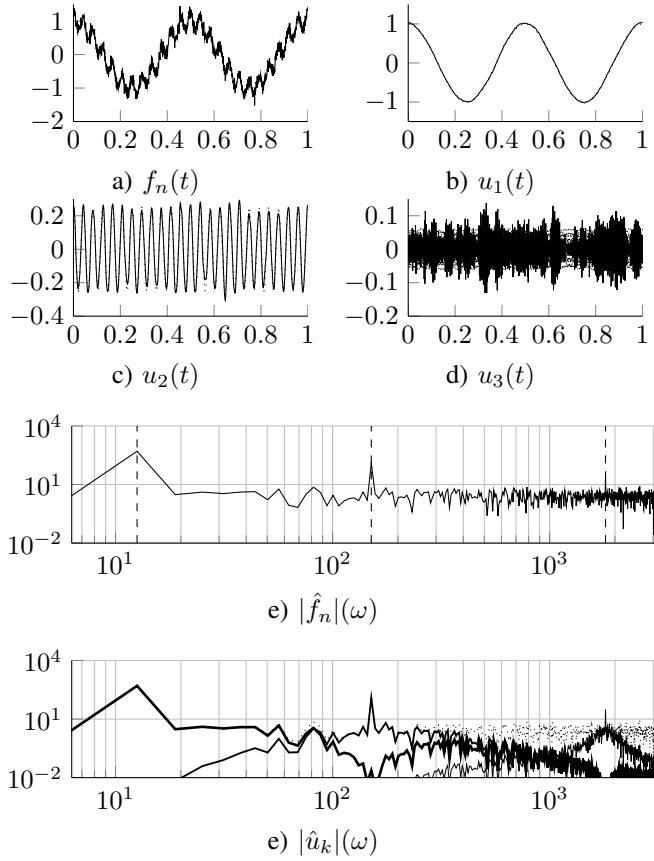


Fig. 4. VMD decomposition of noisy tri-harmonic. (a) The noisy input signal. (b)-(d) The three modes extracted by denoising VMD, and the theoretical mode (dotted). (e) The spectrum of the input signal, and (f) its distribution over the three modes.

### B. Tones separation

The next slightly more complicated challenge is the separation of two different superimposed tones [2]. Here, the input signal is composed of two different, pure harmonics:

$$f_{\nu_1, \nu_2}(t) = a_1 \cos(2\pi\nu_1 t) + a_2 \cos(2\pi\nu_2 t), \quad (33)$$

with  $\nu_2 < \nu_1 < f_s/2$ , and  $a_{1,2}$  two possibly different amplitudes. As a function of the amplitude ratio  $\rho = a_1/a_2$ , EMD exhibits different, important regions of confusion, where the two signals are too close in frequency to be separated correctly, as reported in [2] and illustrated in figure 3.

Again, we apply the same analysis to the proposed VMD model, and again we do not employ any windowing. The results for varying amplitude ratios  $\rho \in \{1/4, 1, 4\}$  are shown in figure 3 along with the corresponding EMD results. As can be clearly seen, the proposed VMD achieves good tones separation over the whole domain except at the Nyquist frequency. In particular, the decomposition quality is not significantly worse for close harmonics.

### C. Noise robustness

To illustrate the VMD robustness with respect to noise in the input signal, we test using the following tri-harmonic signal, affected by noise:

$$f_n(t) = \cos(4\pi t) + \frac{1}{4} \cos(48\pi t) + \frac{1}{16} \cos(576\pi t) + 0.1\eta, \quad (34)$$

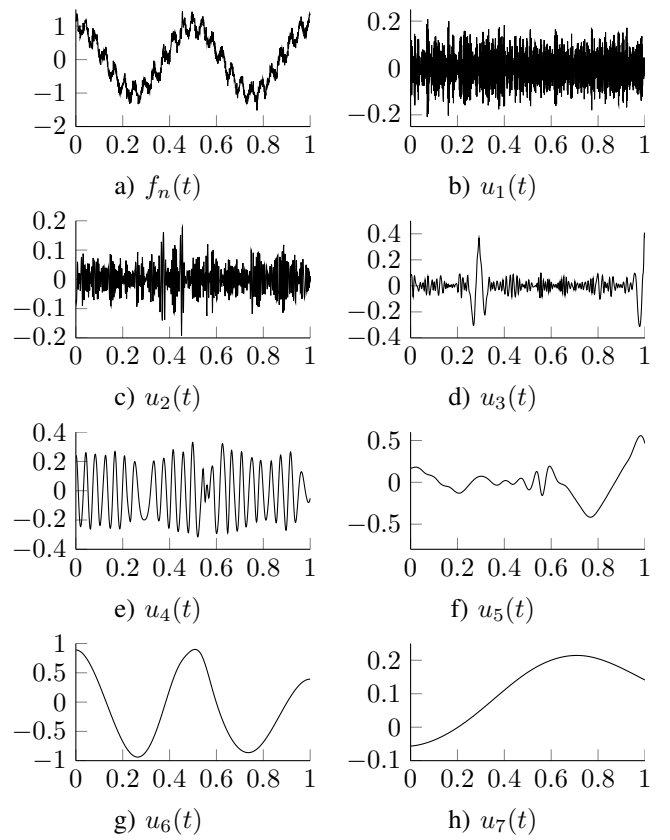


Fig. 5. EMD decomposition of noisy tri-harmonic. (a) noisy input signal. (b)-(h) The seven modes extracted by EMD. None of the modes corresponds to a pure harmonic.

where  $\eta \sim \mathcal{N}(0, 1)$  represents the Gaussian additive noise. The noise level is quite important with respect to the amplitude of the highest harmonic. We perform variational modes decomposition into three modes, without Lagrangian multipliers in order to remove the noise. The signal, and the three components estimated using VMD are shown in Fig. 4. The strong, lowest frequency signal is recovered almost flawlessly. The medium-strength medium-frequency signal is still detected at acceptable quality. The weak, high-frequency signal, however, is difficult. The VMD algorithm correctly tunes the third center-frequency on this harmonic, but the recovered mode is highly affected by the noise. Here, decreasing the bandwidth by increasing  $\alpha$  comes at the risk of not properly capturing the correct center frequency, while too low an  $\alpha$  includes more noise in the estimated mode. The mode could, however, be cleaned further in post-processing. For reference, we note that the estimated VMD center frequencies are off by 0.27%, 1.11% and 0.18% only.

We provide a comparison with EMD<sup>1</sup> based on exactly the same signal in Fig. 5. The EMD produces 7 estimated modes. The first two modes contain the highest-frequency harmonic, and important amounts of noise. The fourth mode comes closest to the middle harmonic, however important features have been attributed to the third and fifth mode. The sixth mode picks up most of the low frequency harmonic, but is severely distorted.

<sup>1</sup>Implementation by Gabriel Rilling, available at <http://perso.ens-lyon.fr/patrick.flandrin/emd.html>

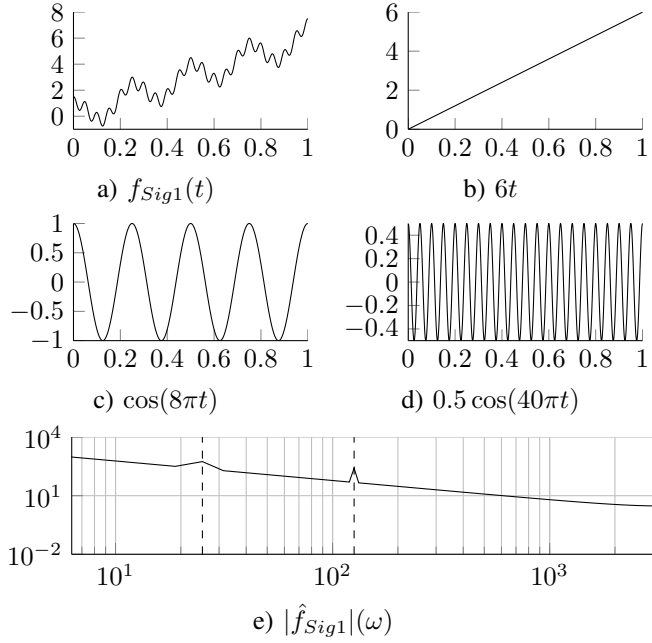


Fig. 6. a)  $f_{Sig1}(t)$ , b–d) its constituent modes. e) The signal’s spectrum.

#### D. Complex multimode signals

Now we look at slightly more complex signals to be decomposed. In particular, we consider the same test signals that were previously suggested in [14] and also used in [12], with the purpose of increased comparability.

1) *Example 1:* The first signal is a composition of three simple components, namely a general linear trend and two different harmonics:

$$f_{Sig1}(t) = 6t + \cos(8\pi t) + 0.5 \cos(40\pi t). \quad (35)$$

The signal, its three constituent modes, and the composite Fourier spectrum are shown in figure 6. The main challenge of this signal is the linear growth term. Without windowing, the higher order harmonics of the periodized sawtooth signal spread over the whole spectrum.

In order to reduce the effects of periodization, we apply Gaussian windowing. The corresponding windowed signal, and the respective VMD results are illustrated in detail in figure 7. In particular, we show how the two non-zero center frequencies  $\omega_2$  and  $\omega_3$  quickly converge towards the exact harmonics. The corresponding modes constitute a nice partition of the input spectrum, with each mode being clearly dominant around its respective center frequency. The three modes in time domain show nice separation into three distinct signals of characteristic oscillations. After “unwindowing” by pointwise division of the estimated modes by the Gaussian window, we recover good estimates of the true underlying modes (dotted lines), valid on the central 60% of the signal.

2) *Example 2:* The second example uses a quadratic trend, a chirp signal, and a third mode with sharp transition between

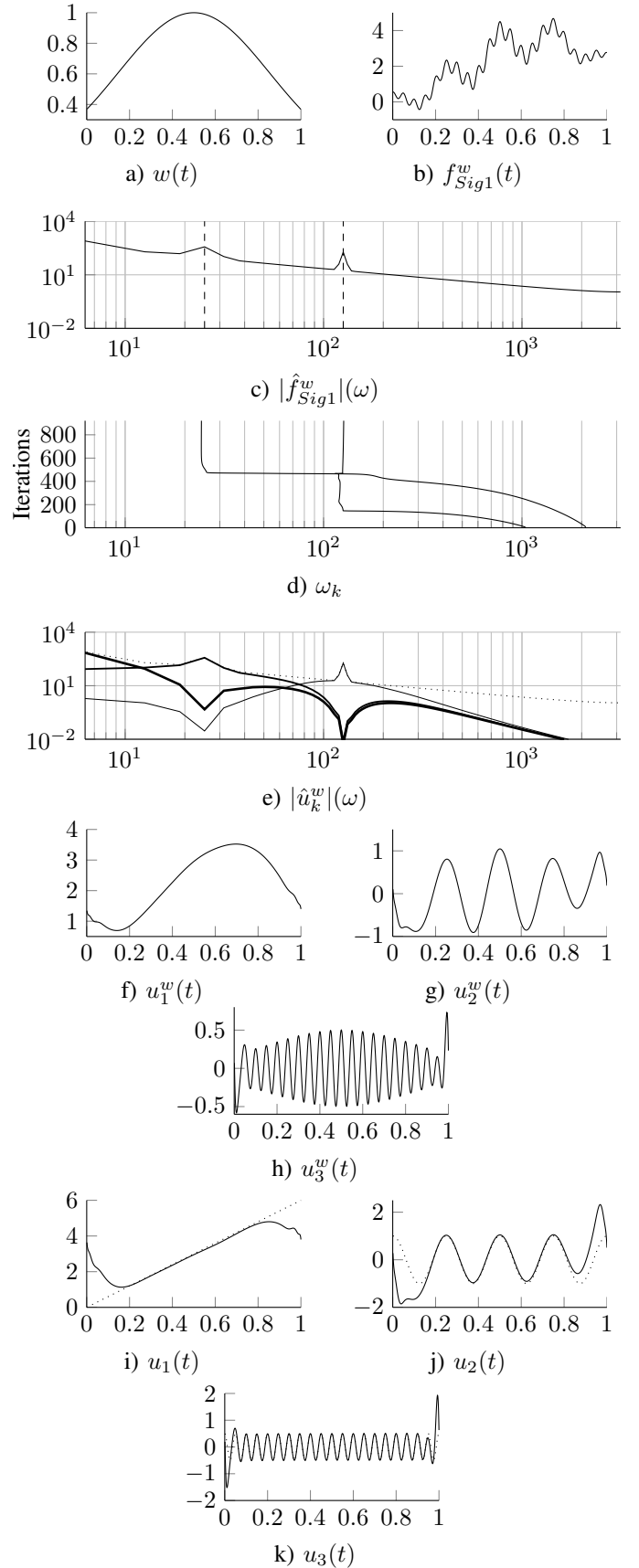


Fig. 7. VMD decomposition of  $f_{Sig1}$ . a) The applied window, b) the windowed signal, and c) its spectrum. d) Evolution of the detected center frequencies, and e) the corresponding spectrum decomposition. f–h) the reconstructed modes prior to, and i–k) after Gaussian window removal.

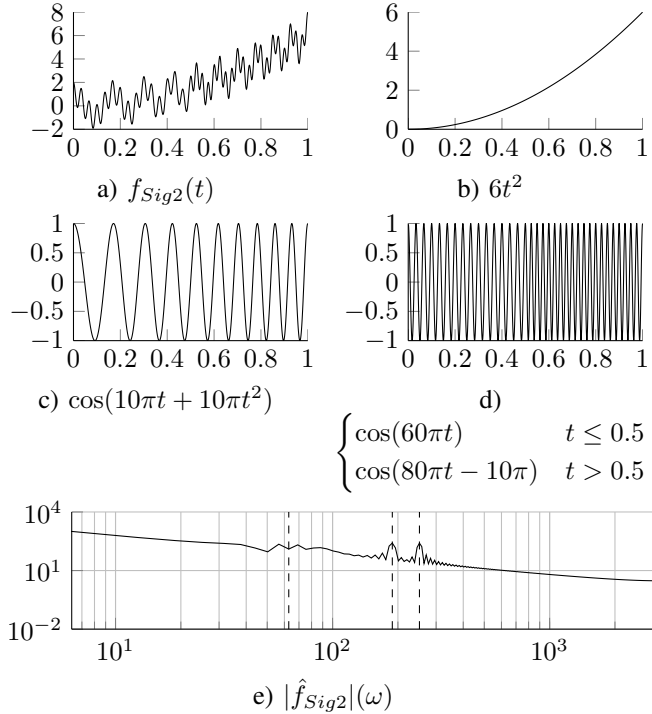


Fig. 8. a)  $f_{Sig2}$ , b–d) its constituent modes. e) The signal’s spectrum.

two constant frequencies<sup>2</sup>:

$$f_{Sig2}(t) = 6t^2 + \cos(10\pi t + 10\pi t^2) + \begin{cases} \cos(60\pi t) & t \leq 0.5 \\ \cos(80\pi t - 10\pi) & t > 0.5 \end{cases} \quad (36)$$

The signal, its three constituent modes, and the composite Fourier spectrum are shown in figure 8. The instantaneous frequency of the chirp is given by the time derivative of its phase:

$$\omega(t) := \partial_t \phi(t) = 10\pi + 20\pi t. \quad (37)$$

Thus, for  $t \in [0, 1]$  the instantaneous frequency varies linearly between  $10\pi$  and  $30\pi$ . Consequently, the theoretical center frequency of the mode is located at  $20\pi$ . The piecewise-constant bi-harmonic has spectral peaks expected at  $60\pi$  and  $80\pi$ .

Here, too, we employ Gaussian windowing to alleviate periodization artifacts. Indeed, the windowed signal has a much cleaner spectrum, and the expected peaks of the signal’s components become more prominent, as illustrated in figure 9. Again, the estimated center frequencies  $\omega_k$  converge to the expected frequencies precisely. Here, we chose to decompose into four modes, thus assigning each half of the piecewise-constant frequency signal to a separate mode. The spectral partitioning can be nicely appreciated in the spectral plot of the different modes. The unwinded mode estimates fit well the theoretical signals, except again for boundary issues.

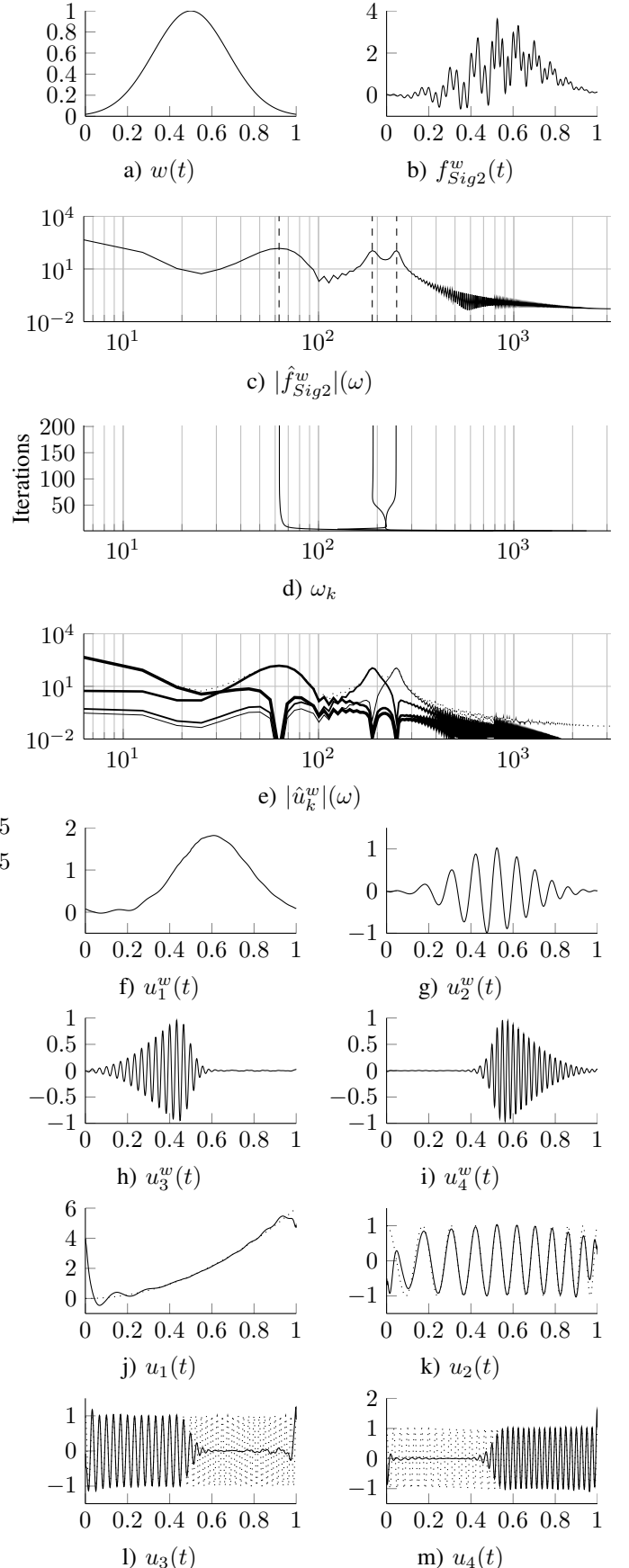


Fig. 9. Results of VMD on  $f_{Sig2}$ . a) The applied window, b) the windowed signal, and c) its spectrum. d) Evolution of the detected center frequencies, and e) the corresponding spectrum decomposition. f–i) the reconstructed modes prior to, and j–m) after Gaussian window removal.

<sup>2</sup>Here, we changed the phase shift in the third component, with piecewise-constant frequency, from  $15\pi$  to  $10\pi$ , in order to have a continuous signal.

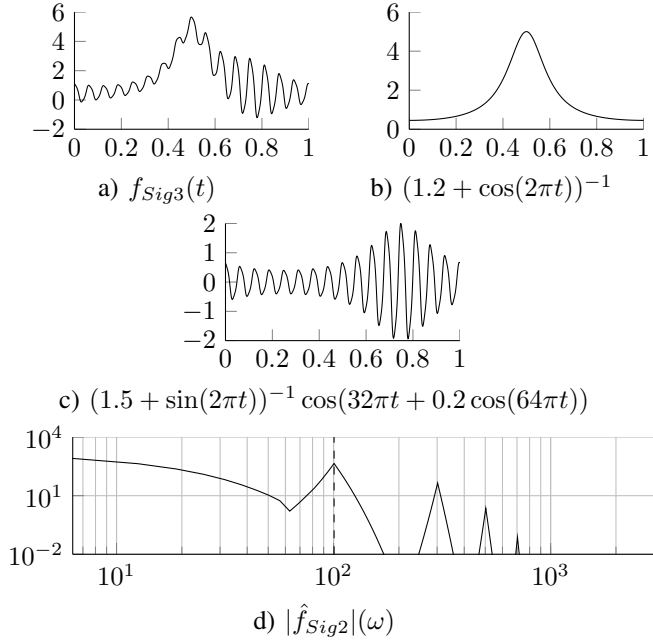


Fig. 10. a)  $f_{Sig3}$ , b-c) its constituent modes. d) The signal's spectrum.

3) *Example 3*: The third synthetic signal has intrawave frequency modulation:

$$f_{Sig3}(t) = \frac{1}{1.2 + \cos(2\pi t)} + \frac{\cos(32\pi t + 0.2 \cos(64\pi t))}{1.5 + \sin(2\pi t)}. \quad (38)$$

The signal, its three constituent modes, and the composite Fourier spectrum are shown in figure 10. While the first, bell-shaped component has mostly low-pass content, the second mode's main peak is clearly identified at  $32\pi$ . However, due to the non-linear intrawave frequency modulation, an important amount of higher-order harmonics are also observed at  $32\pi + 64\pi = 96\pi$ ,  $32\pi + 2 \cdot 64\pi = 160\pi$  and  $32\pi + 3 \cdot 64\pi = 224\pi$ , respectively. This second component obviously violates the narrowband assumption, and one would naturally expect some difficulties recovering this mode using VMD. Indeed, by Carson's rule, the mode's bandwidth here is dominantly controlled by the relatively high frequency of the modulating term  $\cos(64\pi t)$ , essentially spreading the mode over the whole practical spectrum.

The slightly windowed signal and the corresponding VMD results are illustrated in figure 11. The non-zero  $\omega_2$  quickly converges to the correct main frequency  $32\pi$ . The higher order harmonics are not uniquely attributed to the second mode, but shared between both modes. Consequently, the intrawave frequency modulation is shared by both modes, creating some ripples in the otherwise low-frequency mode. Nonetheless, the reconstructed estimated modes fit well the constituent signals (dotted lines). Most of the error occurs at the boundaries, and at the very center of the signal, where the low-frequency mode has a sharp peak, involving some higher frequency features wrongly attributed to the higher-frequency mode.

4) *Example 4*: The fourth example is a real signal from an electrocardiogram (ECG), data shared by [12]. These data present numerous components, as seen in figure 12. Beyond

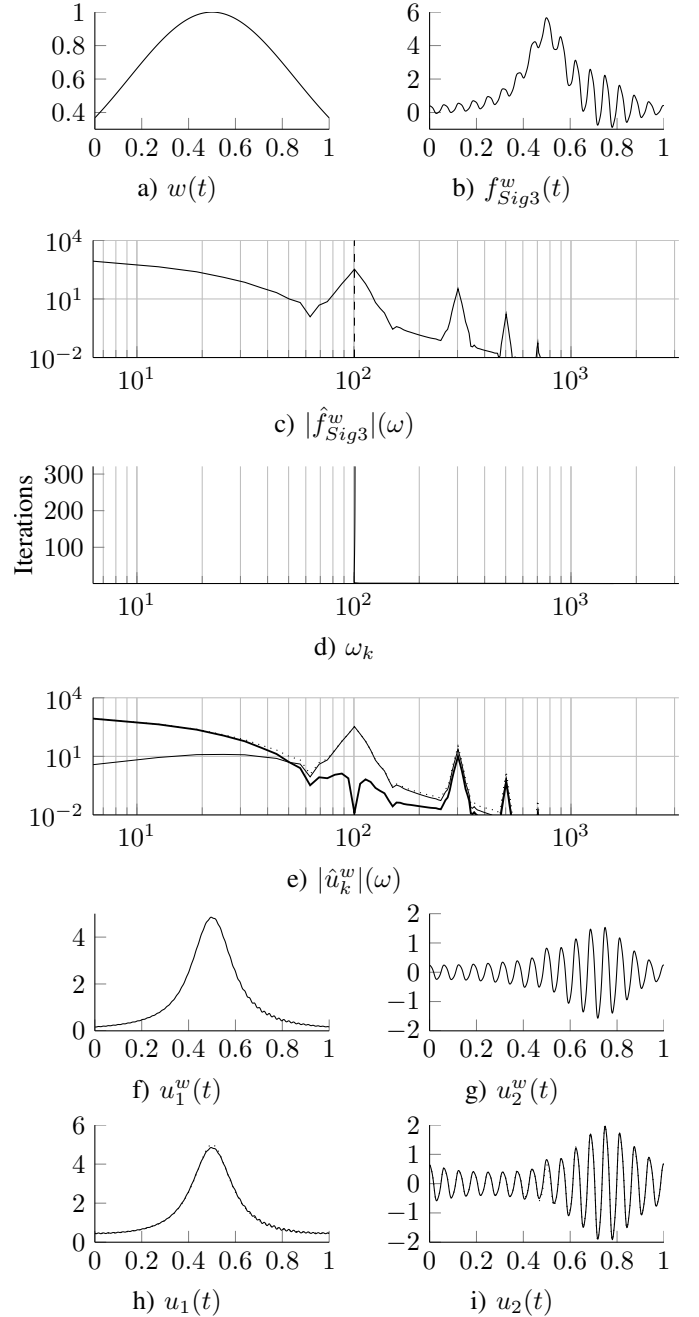


Fig. 11. Results of VMD on  $f_{Sig3}$ . a) The applied window, b) the windowed signal, and c) its spectrum. d) Evolution of the detected center frequencies, and e) the corresponding spectrum decomposition. f-g) the reconstructed modes prior to, and h-i) after Gaussian window removal.

the expected spikes-train driven by the rhythm of the heartbeat, one can clearly see an oscillating low-frequency pattern. At the other end of the spectrum, there is distinct high-frequency noise at a single high-pitch harmonic, most likely the electric power-line frequency. The distinct spikes of the ECG signal create important higher-order harmonics.

The spectrum after slight Gaussian windowing, and the results of VMD are depicted in figure 13. We chose a high-number of 10 modes to be detected, to accommodate the numerous higher-order harmonics of the spikes. The respective center frequencies nicely converge to these spectral peaks. The

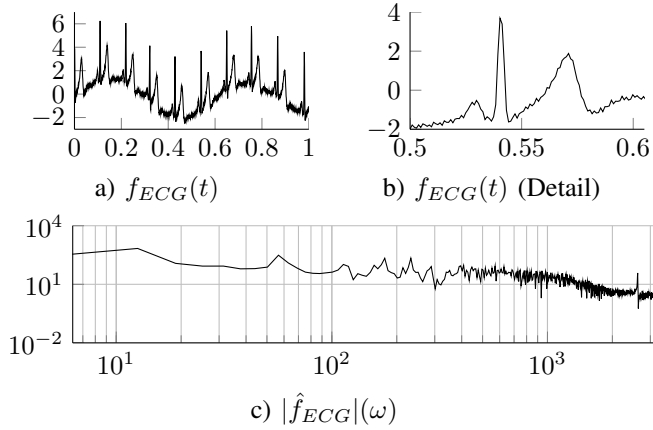


Fig. 12. a) ECG signal 7. b) Detail. c) The signal's spectrum.

first, low-frequency mode captures the low-frequency oscillation of the baseline. The highest frequency mode contains the most noise. The first actual ECG specific mode oscillates precisely at the frequency of the heartbeat. The higher ECG modes then contain the higher-order wave-packets around the highly non-sinusoidal spikes. A “clean” ECG signal can be reconstructed by summing all but the first and last VMD modes, thus discarding the low-frequency baseline oscillation and most of the high-frequency noise.

## V. CONCLUSIONS AND OUTLOOK

In this paper, we have presented a novel variational method for decomposing a signal into an ensemble of band-limited intrinsic mode functions, that we call Variational Mode Decomposition, (VMD). In contrast to existing decomposition models, like the empirical mode decomposition (EMD), we refrain from modeling the individual modes as signals with explicit IMFs. Instead, we replace the most recent definition of IMFs, namely their characteristic description as AM-FM signals, by the corresponding narrow-band property. Indeed, we provide a formula that relates the parameters of the explicit AM-FM descriptors to the estimated signal bandwidth.

Our decomposition model solves the inverse problem as follows: decompose a signal into a given number of modes, either exactly or in a least squares sense, such that each individual mode has limited bandwidth. We assess the mode's bandwidth as the squared H1 norm of its Hilbert complemented analytic signal with only positive frequencies, shifted to baseband by mixing with a complex exponential of the current center frequency estimate. The variational problem is solved very efficiently in a classical ADMM approach: The modes are updated by simple Wiener filtering, directly in Fourier domain with a filter tuned to the current center frequency, then the center frequencies are updated as the center of gravity of the mode's power spectrum, and finally the Lagrangian multiplier enforcing exact signal reconstruction is updated as dual ascent.

In our experiments, we show that the proposed VMD scheme clearly outperforms EMD with regards to tone detection, tone separation, and noise robustness. Further, we apply our model to more complicated signals for comparison

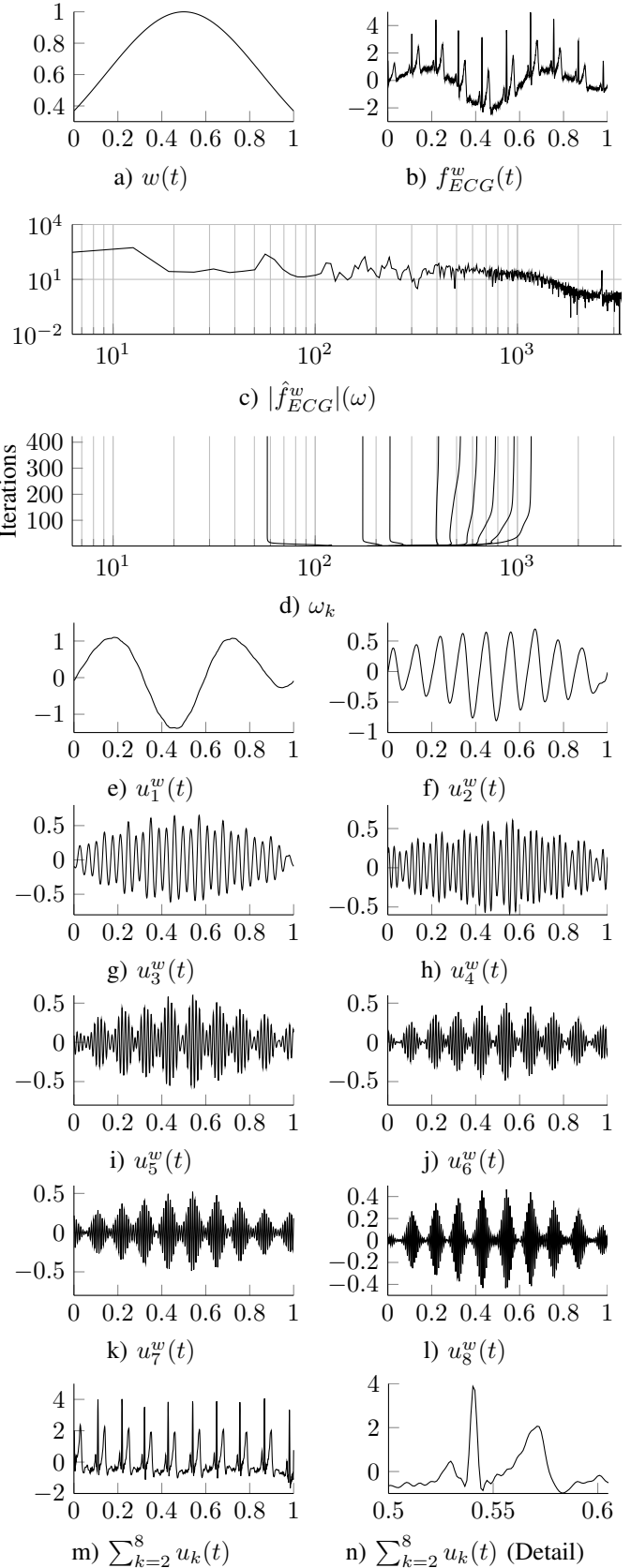


Fig. 13. Results of ECG signal 7. a) The applied window, b) the windowed signal, and c) its spectrum. d) Evolution of the detected center frequencies. e–l) The reconstructed modes prior to Gaussian window removal. m) Cleaned ECG, and n) detail.

with other state-of-the-art methods, and can show successful decomposition.

The most important limitation of the proposed VMD is with boundary effects, and sudden signal onset in general. This is strongly related to the use of an L2-based smoothness term, that overly penalizes jumps at the domain borders and within; conversely, this is also reflected by implicit periodicity assumptions when optimizing in Fourier domain, and by the narrow-band violation caused by discontinuous envelopes in such AM-FM signals. Another point that critics might highlight, is the required explicit (manual) selection of the number of active modes in the decomposition, like in EWT but as opposed to EMD. Current work addresses these shortcomings, and we are also working on suitable extensions to signals on domains of dimension greater than one.

#### ACKNOWLEDGMENTS

The authors gratefully acknowledge valuable discussions with and input from: Prof. A. L. Bertozzi, Dr. J. Gilles, and Dr. Y. van Gennip.

#### REFERENCES

- [1] N. E. Huang, Z. Shen, S. R. Long, M. C. Wu, H. H. Shih, Q. Zheng, N.-C. Yen, C. C. Tung, and H. H. Liu, "The empirical mode decomposition and the Hilbert spectrum for nonlinear and non-stationary time series analysis," *Proceedings of the Royal Society A: Mathematical, Physical and Engineering Sciences*, vol. 454, no. 1971, pp. 903–995, Mar. 1998.
- [2] G. Rilling, P. Flandrin, and P. Gonçalvès, "On empirical mode decomposition and its algorithms," in *IEEE-EURASIP workshop on Nonlinear Signal and Image Processing*, 2003.
- [3] G. Rilling and P. Flandrin, "One or Two Frequencies? The Empirical Mode Decomposition Answers," *IEEE Transactions on Signal Processing*, vol. 56, no. 1, pp. 85–95, Jan. 2008.
- [4] P. Flandrin, P. Gonçalvès, and G. Rilling, "EMD equivalent filter banks, from interpretation to applications," in *Hilbert-Huang Transform and Its Applications*, 2005, pp. 57–74.
- [5] N. Klügel, "Practical Empirical Mode Decomposition for Audio Synthesis," in *Int. Conference on Digital Audio Effects (DAFx-12)*, no. 2, 2012, pp. 15–18.
- [6] B. Barnhart and W. Eichinger, "Empirical Mode Decomposition applied to solar irradiance, global temperature, sunspot number, and CO2 concentration data," *Journal of Atmospheric and Solar-Terrestrial Physics*, vol. 73, no. 13, pp. 1771–1779, Aug. 2011.
- [7] S. Assous, A. Humeau, and J.-P. L'huillier, "Empirical mode decomposition applied to laser Doppler flowmetry signals : diagnosis approach." *IEEE Engineering in Medicine and Biology Conference (EMBC)*, vol. 2, pp. 1232–5, Jan. 2005.
- [8] A. O. Andrade, S. Nasuto, P. Kyberd, C. M. Sweeney-Reed, and F. Van Kanijn, "EMG signal filtering based on Empirical Mode Decomposition," *Biomedical Signal Processing and Control*, vol. 1, no. 1, pp. 44–55, Jan. 2006.
- [9] S. Liu, Q. He, R. X. Gao, and P. Freedson, "Empirical mode decomposition applied to tissue artifact removal from respiratory signal." *IEEE Engineering in Medicine and Biology Conference (EMBC)*, pp. 3624–3627, Jan. 2008.
- [10] I. Mostafanezhad, O. Boric-Lubecke, V. Lubecke, and D. P. Mandic, "Application of empirical mode decomposition in removing fidgeting interference in doppler radar life signs monitoring devices," *IEEE Engineering in Medicine and Biology Conference (EMBC)*, pp. 340–343, Jan. 2009.
- [11] I. Daubechies, J. Lu, and H.-T. Wu, "Synchrosqueezed wavelet transforms: An empirical mode decomposition-like tool," *Applied and Computational Harmonic Analysis*, vol. 30, no. 2, pp. 243–261, Mar. 2011.
- [12] J. Gilles, "Empirical Wavelet Transform," *IEEE Transactions on Signal Processing*.
- [13] J. Carson, "Notes on the Theory of Modulation," *Proceedings of the IRE*, vol. 10, no. 1, pp. 57–64, Feb. 1922.
- [14] T. Y. Hou and Z. Shi, "Adaptive Data Analysis via Sparse Time-Frequency Representation," *Advances in Adaptive Data Analysis*, vol. 03, no. 1 & 2, pp. 1–28, Apr. 2011.
- [15] M. Feldman, "Time-varying vibration decomposition and analysis based on the Hilbert transform," *Journal of Sound and Vibration*, vol. 295, no. 3–5, pp. 518–530, Aug. 2006.
- [16] H.-T. Wu, P. Flandrin, and I. Daubechies, "One or Two Frequencies? the Synchrosqueezing Answers," *Advances in Adaptive Data Analysis*, vol. 03, no. 01n02, pp. 29–39, Apr. 2011.
- [17] M. Bertero, T. A. Poggio, and V. Torre, "Ill-Posed Problems in Early Vision," in *Proceedings of the IEEE*, vol. 76, no. 8, 1988, pp. 869–889.
- [18] A. N. Tichonov, "Solution of incorrectly formulated problems and the regularization method," *Soviet Mathematics*, vol. 4, pp. 1035–1038, 1963.
- [19] V. A. Morozov, "Linear and nonlinear ill-posed problems," *Journal of Mathematical Sciences*, vol. II, no. 6, pp. 706–736, 1975.
- [20] N. Wiener, *Extrapolation, Interpolation, and Smoothing of Stationary Time Series*, 1949.
- [21] R. C. Gonzalez and R. E. Woods, *Digital Image Processing*. Addison Wesley, 1992.
- [22] M. Unser, D. Sage, and D. Van De Ville, "Multiresolution Monogenic Signal Analysis Using the Riesz Laplace Wavelet Transform," *IEEE Transactions on Image Processing*, vol. 18, no. 11, pp. 2402–2418, 2009.
- [23] S. L. Hahn, *Hilbert transforms in signal processing*. Artech House, Inc., 1996.
- [24] D. Gabor, "Theory of Communication," *Journal of the Institution of Electrical Engineers - Part III: Radio and Communication Engineering*, vol. 93, no. 26, pp. 429–457, 1946.
- [25] D. P. Bertsekas, "Multiplier methods: A survey," *Automatica*, vol. 12, no. 2, pp. 133–145, 1976.
- [26] J. Nocedal and S. J. Wright, *Numerical optimization*, 2nd ed. Springer, Berlin, 2006.



**Konstantin Dragomiretskiy** received the B.S. (Hons.) degree in mathematics and the B.A. degree in economics from the University of California, San Diego, CA, USA, in 2010.

He was an Intern Researcher at Sun Microsystems, Menlo Park, CA, USA, in 2006, and an Undergraduate Researcher at California State University, Chico, CA, USA, in 2008. He is currently a Research Assistant at the Department of Mathematics at the University of California, Los Angeles, CA, USA, working towards his Ph.D.

degree with Prof. Andrea L. Bertozzi. His current research interests include variational and PDE based methods applied to signal and image processing problems.



**Dominique Zosso** (S'06–M'11) received the M.Sc. degree in electrical and electronics engineering and the Ph.D. degree from École Polytechnique Fédérale de Lausanne (EPFL), Lausanne, Switzerland, in 2006 and 2011, respectively.

He was a Researcher with the Structural Bioinformatics Group at the Swiss Institute of Bioinformatics and Biozentrum, University of Basel, Basel, Switzerland, from 2006 to 2007. He was Research and Teaching Assistant at the Signal Processing Laboratory, EPFL, from 2007 to 2012. He is currently

a Post-Doctoral Scholar with the Department of Mathematics, University of California, Los Angeles, CA, USA, with Luminita A. Vese, Andrea L. Bertozzi and Stanley J. Osher. His current research interests include PDE and variational models for inverse problems in computer vision, signal and image processing, and efficient algorithms to solve them.